Journal of Biomedical Materials Research Part A

Improved cell infiltration of electrospun nanofiber mats by periodic modulation of fiber density and spatial organization for layered tissue constructs

Journal:	*Journal of Biomedical Materials Research: Part A*
Manuscript ID	JBMR-A-15-0866
Wiley - Manuscript type:	Original Article
Date Submitted by the Author:	28-Nov-2015
Complete List of Authors:	Mahjour, Seyed; Stevens Institute of Technology, Biomedical Engineering, Chemistry and Biological Sciences Sefat, Farshid; Stevens Institute of Technology, Biomedical Engineering, Chemistry and Biological Sciences Polunin, Yevgeniy; Stevens Institute of Technology, Biomedical Engineering, Chemistry and Biological Sciences Wang, Lichen; Stevens Institute of Technology, Biomedical Engineering, Chemistry and Biological Sciences Wang, Hongjun; Stevens Institute of Technology, Chemistry, Chem Biol & Biomedical Engr
Keywords:	cell infiltration, polycaprolactone (PCL), collagen, nanofiber, layered tissue constructs

Title: Improved cell infiltration of electrospun nanofiber mats by periodic modulation of fiber density and spatial organization for layered tissue constructs

Seyed Babak Mahjour (M.D., M.E.)[#], Farshid Sefat (Ph.D.)[#], Yevgeniy Polunin (B.S.), Lichen Wang (M.S.), and Hongjun Wang (Ph.D.)*

Department of Biomedical Engineering, Chemistry and Biological Sciences, Stevens Institute of Technology, Hoboken, New Jersey 07030, U.S.A.

# Equal contribution

*Corresponding Author:

Dr. Hongjun Wang

Department of Biomedical Engineering, Chemistry, Biological Sciences

Stevens Institute of Technology

McLean Hall, Room 416

Hoboken, New Jersey 07030, USA.

E-mail: hongjun.wang@stevens.edu

Tel: (+1) 201.216.5556

Running title: Improved cell infiltration within periodically organized nanofibers

Abstract

While achieving the spatial organization of cells within 3D assembled nanofiber/cell constructs *via* nanofiber-enabled cell layering, the small sizes of inter-fiber pores of the electrospun nanofiber mats could significantly limit cell penetration across the layers for rapid formation of an integrated tissue construct. To address this challenge, efforts were made to improve cell-infiltration of electrospun nanofiber mats by modulating the density distribution and spatial organization of the fibers during electrospinning. Collection of collagen-containing electrospun nanofibers (300-600 nm in diameter) onto the surface of a stainless steel metal mesh (1 mm × 1 mm in mesh size) led to the periodic alternation of fiber density from densely packed to loosely arranged distribution within the same mat, in which the densely packed fibers maintained the structural integrity while the region of loose fibers allowed for cell penetration. Along with improved cell infiltration, the distinct fiber organization between dense and loose fiber regions also induced different morphology of fibroblasts (stellate *vs*. elongated spindle-like). Assembly of cell-seeded nanofiber sheets into 3D constructs with such periodically organized nanofiber mats further demonstrated their advantages in improving cell penetration across layers in comparison to either random or aligned nanofiber mats. Taken together, modulation of nanofiber density to enlarge the pore size is effective to improve cell infiltration through electrospun mats for better tissue formation.

Keywords: layered tissue constructs, cell infiltration, polycaprolactone (PCL), collagen, nanofibers

1. Introduction

Many tissues in our body take the multilayered structure with varying cell types or tissue matrix to fulfill the unique physiological functions, e.g., the two distinct compartments of skin can effectively minimize dehydration and microorganism invasion via the tight outermost epidermis while tuning the temperature and sensing the surroundings with sweat glands and nerve endings in the dermis [1, 2]. In recognition, efforts have been made to recapitulate such laminated structures in tissue-engineered constructs [3-7]. In alignment with such efforts, we also develop a nanofiber-assisted cell assembly strategy, in which cell seeding and electrospinning are alternated to form 3D constructs [8]. The use of electrospun fibers, normally in the diameter range of tens to hundreds of nanometers, offers the opportunity to recapture the key morphological and dimensional characteristics of extracellular matrix (ECM) of native tissues [9,10]. While successfully demonstrating the efficiency of such an approach in forming multilayered tissues [8, 11], however, the intrinsic small inter-fiber pore sizes (normally less than 5 μm), especially for those matrices with randomly oriented fibers, would limit cell penetration across the layers to form integrated tissues and meanwhile constrain cell migration in and out of the constructs for further integration with host tissue upon in vivo implantation. In this regard, attempts have been made to improve the porosity and increase the pore size of electrospun matrices by using sacrificial microbeads, particulate leaching or freeze-drying [12-17], which can help to improve tissue ingrowth, but may not be suitable for creating large pores through rather thin (typically in 10 to 20 μm) nanofiber mats for layering. To this end, establishment of a cost-effective strategy to improve cell penetration yet maintain the structural integrity and dimensional superiority of nanofiber mats will be highly desired [18, 19].

During electrospinning, a grounded conductive surface is normally used to collect the electrospun nanofibers. In the course of fiber collection, it is possible to manipulate the distribution of electric fields for achieving unique spatial organization of fibers to accommodate the anisotropy of native ECM [20], *e.g.*, fibers collected on a rotatory mandrel exhibit an orientation parallel to the rotating direction [21]. In addition, intervention of electric field distribution by using a patterned collection surface can correspondently affect fiber deposition to introduce unique fiber organization within electrospun mats [22-24]. Studies have shown that such patterned fiber mats can yield better mechanical strength and induce distinctive cellular responses on their surface [25, 26]. However, it is unclear whether such electrical field-induced modulation of fiber organization can effectively increase the inter-fiber distance for cell infiltration. Thus, the primary focus of this study was to determine whether periodic modulation of fiber distribution and organization within the electrospun nanofiber mats could achieve high cell penetration and consequently facilitate the formation of integrated tissue constructs using the nanofiber-enabled cell layering technology [8, 11].

To better support the adhesion and proliferation of cells, a polyblend of collagen and polycaprolactone (PCL) was used to fabricate the nanofibers. The morphology and pore size of mesh-patterned nanofiber mats were microscopically characterized and cell infiltration was evaluated by counting the pass-through cells. Besides, patterned PCL/collagen nanofiber mats were also used to layer-by-layer assemble fibroblasts to form 3D constructs with a special emphasis on cell migration and layer fusion for structural integrity in comparison with those nanofiber mats with either only randomly or only uniaxially oriented fibers.

2. Materials and Methods

2.1. Materials

1,1,1,3,3,3-hexafluoro-2-propanol (HFIP) was obtained from Oakwood products Inc (West Columbia, SC). Poly(epsilon-caprolactone) (PCL, Mw=80,000) was purchased from Sigma-Aldrich (St. Louis, MO) and type I collagen (collagen) was obtained from Elastin Products Inc. (Owensville, MO). All other reagents and solutions were obtained from Invitrogen (Grand Island, NY) except as indicated.

2.2 Cell isolation and culture

Following the modified cell isolation protocols [27], dermal fibroblasts were isolated from the dorsal skin of Sprague Dawley rat (female, 250-300 gram, Charles River) with approval from the Institutional Animal Care and Use Committee. Briefly, the shaved rat skin (1 cm × 1 cm) was harvested, cleaned and then incubated with 0.25% dispase II solution for 30-60 min to separate the epidermis from dermis. Fibroblast cells were isolated by incubating the minced dermal pieces (~1 mm in size) with 0.75% collagenase I (Sigma-Aldrich, Saint Louis, MO) and 0.25% dispase II for 2 hrs. Fibroblasts were cultured in Dulbecco's modified Eagle medium (DMEM) with 10% fetal bovine serum (FBS) (ATCC, Manassas, VA) and 1% penicillin/streptomycin (P/S) and subcultured upon reaching 70-80% confluence.

2.3 Preparation of electrospun nanofiber mats

Electrospun PCL/collagen nanofibers were prepared using our established electrospinning protocol [20]. Briefly, a homogeneous mixture of PCL (8.0% w/v) and Type I collagen (8.0% w/v) dissolved in HFIP at a ratio of 3:1 was loaded into 5-mL syringe (Becton Dickinson, Franklin Lakes, NJ) with a tip-blunt capillary (0.9 mm of the internal diameter). Under the optimized electrospinning conditions, *i.e.*, a constant feed rate of 0.6 mL/hr, a voltage of 10-15 kV, and a collection distance of 10 cm, PCL/collagen nanofibers were collected onto various grounded surfaces for different fiber organizations. Onto a stationary solid conductive surface

were randomly organized nanofiber mats obtained (Fig. 4A). Onto a rotatory conductive mandrel surface were aligned fiber mats obtained (Fig. 4B) [21]. Onto a stationary stainless steel wire mesh (see Fig. 1A) with the mesh size of 1 mm × 1 mm were mesh-patterned fiber mats obtained. All electrospun nanofiber mats were collected on the rings with a diameter of 2.54 cm and sterilized by UV irradiation for 30 min prior to further use.

2.4 Microscopic characterization of nanofiber mats

The overview of prepared PCL/collagen fiber mats was visualized under the Micromaster™ inverted digital microscopes (Fisher Scientific, Pittsburg, PA). The fiber diameter, morphology and pore size were further characterized by scanning electron microscopy (SEM). Upon sputter coating with Au/Pd alloy (MED020, Leica Microsystems), the fiber mats were examined using the Auriga FIB-SEM (Zeiss, Peabody, MA). Images from 5 randomly selected areas were captured and used for further analyses of fiber diameter and pore size using ImageJ1.49 (NIH).

2.5 Mechanical test

The tensile strength of mesh-patterned nanofiber mats with electrospinning time of 10 to 40 sec was determined. Briefly, the samples were cut into rectangles with the dimension of 1.0 cm × 3.0 cm. Mechanical testing was performed on a Materials Testing System (MTS-858-BIONIX, USA) with an initial tension preload of 1 N. Tensional loads were applied to each specimen at a constant strain rate of 0.5 mm/s until a maximum deformation of 5 mm was reached. A total number of five specimens were used for each experimental condition.

2.6 Simulation of electric field using COMSOL Multiphysics

To help understanding the correlation between electric field distribution and nanofiber organization, COMSOL Multiphysics 4.4 was used to simulate the potentials of electric field within our established electrospinning setup. Solid works 2013 was used to draw the stainless

steel metal wire mesh array in four directions, and then it was imported into the COMSOL Multi-physics module for electric field distribution.

2.7 Cell seeding onto nanofiber mats and bottom-up assembly into 3D layered constructs

Rat dermal fibroblasts (passage 1-2), after trypsinization and resuspension in the media at a final concentration of 4×10^5 cells/mL, were seeded onto electrospun fiber mats. To characterize the capability of cell infiltration through the nanofiber mats, cells that passed through the mat and deposited on the bottom of petri dish were collected and counted (n=5 per condition). Cell-seeded nanofiber mats were either continuously cultured for cell morphology evaluation, or assembled into 3D constructs following the layer-by-layer stacking manner (see Fig. 7A). Totally, 15 layers of cell-seeded nanofiber mats were assembled in this study. The assembled constructs were further cultured in fibroblast media (DMEM supplemented with 10% FBS and 1% P/S).

2.8 Histological analysis

For histologic analyses, the constructs cultured for 14 days were harvested and fixed in 4% paraformaldehyde fixative for 1 hr at room temperature. Upon dehydration in a series of graded ethanol solutions until 100% ethanol, the constructs were then embedded and cut into thin sections (7 μm thick). Cross-sections stained with hematoxylin and eosin (H&E) (Sigma) were examined under a Nikon 80i upright microscope. Representative images were captured and analyzed by the analysis software (NIS-elements BR 3.10, Nikon, Japan) to evaluate cell infiltration through the electrospun fiber layers.

2.9 Methylene blue staining and fluorescence staining

The overview of fibroblasts cultured on various nanofiber mats was evaluated by methylene blue staining and then examined under a Nikon stereomicroscope as previously described [28]. To better visualize the cell morphology, fluorescence staining for F-actin was also performed to the

culture. Briefly, cultured cells were fixed in 4% paraformaldehyde for 10 min and then incubated with phalloidin-TRITC (Biotium, 1:500). Cell nuclei were stained with DAPI (Sigma, 1:1000). The staining was examined under a Nikon 80i epifluorescence microscope.

2.10 Statistical Analysis

Each experiment was repeated at least 3 times and data were expressed as the mean ± SD. An unpaired student t-test was used to evaluate the significance among experimental groups. A value of $p<0.05$ was considered statistically significant.

3. Results

3.1 Fabrication of nanofiber mats with periodic fiber density and organization

To predict the deposition of electrospun PCL/collagen nanofibers onto metal mesh surfaces, COMSOL simulation of the electric potential distribution between spinneret (highest) and metal mesh (lowest) was performed (Fig. 1C). As noted, the potential across the metal mesh surface was not even and a higher potential difference was seen between the spinneret and metal wires, especially those protruded ones (Fig. 1D), suggesting the high chance for fibers to deposit onto these regions. Indeed, electrospun PCL/collagen (3:1, w/w) nanofibers collected onto the stainless steel mesh surface exhibited distinct distribution and organization patterns (Fig. 2A). Three main zones (protruded wire, dented wire and inter-wire void space) were identified. Random and packed nanofibers were collected onto the protruded wires (Fig. 2D) and highly parallel (Fig. 2B and 2C) fibers were seen on the dented wire area. Nanofibers collected onto the inter-wire void space showed some cross-alignment (especially in the center) with a lower fiber density (Fig. 2E). Quantification of the pore size of various zones using Image J revealed the large pores (19.3 ± 1.8 μm) in the inter-wire void space while much smaller pores (less than 3 μm) on the protruded metal wires (Table 1). To determine the optimal thickness for both cell

penetration and mechanical strength, nanofiber mats collected for different electrospinning durations were evaluated for pass-through cells and mechanical strength. With the extension of electrospinning time from 10 to 30 sec, an increase of fiber density over the void space was observed but much less pronounced than that on the metal wires (Fig. 3), maintaining relatively large pore size (Table 2). However, further extending the electrospinning time to 40 sec, the pore size was dramatically reduced with a rather dense fiber density (Fig. 3D, H&L). Cell pass-through study showed that the cell number decreased over the increase of spinning time and a significant reduction of cell pass-through was observed for the spinning time above 30 sec, correlating well with the decrease of pore size. On the other hand, the increase of spinning time could improve the mechanical strength of electrospun mats, reaching as high as 7.0 ± 0.2 MPa for the 40-sec mats. However, the increase of strength was not in a linear proportion to the electrospinning time and around 30 sec was the turning point for plateau (see Supplementary Fig. 1). To keep a high cell pass- through efficiency while maintaining the mechanical strength, nanofiber mats with the spinning time of 25 sec were particularly selected for use in the rest of the experiments.

3.2 Electrospun fiber mats with distinct fiber organizations and their regulation of cell morphology

To identify the difference of mesh-patterned fiber mats from those commonly used ones (*i.e.,* randomly or uniaxially oriented mats), three types of electrospun fiber mats with the same spinning time (25 sec) were fabricated and compared (Fig. 4). Again, the mesh-patterned nanofiber mats showed the largest pore size with the highest cell pass-through capacity (Table 3). To determine the effect of fiber organizations on the morphology of fibroblasts, cells were seeded and cultured on various fiber mats for up to 7 days and then stained with methylene blue

for an overview of cell distribution and with TRITC-phalloidin for cell morphology. Different from even cell distribution on random or aligned fiber mats (Fig. 5A&B), cells on the mesh-patterned mats showed periodic distribution and were dominantly located in the void space (Fig. 5C), indicating that cell attachment and spreading was not completely correlated with fiber density. In addition, cells on the mesh-patterned fiber mats displayed two distinct cell morphologies: on the protruded wire area with random fibers cells showed the stellate morphology (Fig. 5F), similar to those on the random nanofiber mats (Fig. 5D); on the void area with cross-aligned fibers cells became elongated with the orientation closely following the fiber organization (Fig. 5G), but still different from those on the purely aligned fibers (Fig. 5E).

3.3 Formation of 3D layered constructs with nanofiber-assisted bottom-up cell assembly

To further elaborate the advantages of wire mesh-patterned nanofiber mats in cell infiltration through the nanofiber mats for forming thicker tissues, multiple layers of nanofiber mats were stacked with a final thickness of about 100 μm and then seeded fibroblasts from the top as indicated in Fig. 6A. After cultured for 14 days, significant infiltration of fibroblasts into the layers was observed only with the mesh-patterned nanofiber mats (Fig. 6D) and reached about 35.4 ± 8.8 μm in depth in contrast to the limited cell infiltration with either random fiber (2.2 ± 0.5 μm) or aligned fiber mats (4.1 ± 0.7μm) (Table 4). Layer-by-layer stacking of cell-seeded nanofiber mats into a multilayered structure allows the creation of 3D layered constructs with controlled cell density for each layer and their spatial distribution across the entire construct (Fig. 7A). Nanofiber mats (25-sec spinning time with the thickness of 8-10 μm) with random, aligned or mesh-patterned fiber organizations were seeded with fibroblasts and then respectively stacked into 15-layered structures. After culture for 14 days, cross-sections of the constructs were stained with H&E for cell distribution and morphology. It was found that fibroblasts in the constructs

with random fiber mats or aligned fiber mats had a uniform cell distribution throughout the layers but mainly remained within their fiber mat layers (*i.e.*, parallel to the fiber layers), and a majority of cell nuclei elongated parallel to fiber layers (Fig. 7B&C). Interestingly, the cell nuclei of fibroblasts within mesh-patterned fiber/cell constructs showed their elongation, however a majority of them oriented vertical to the fiber layers and crossed various layers (Fig. 7D). Some cells migrated down to the lower portion of the construct, as indicated by arrows in Fig. 7D.

4. Discussion

Recapture of the key morphological features of native ECM is believed to play an important role in regulating appropriate cell phenotype for functional tissue formation [29-31]. Layer-by-layer assembly of cells together with biomimetic nanofibers into 3D constructs (Fig. 7A) allows for the formulation of a specific microenvironment for cells while creating the layered tissue constructs [8]. To facilitate cell migration through the fiber layers, spatial modulation of fiber distribution and density within electrsopun mats as described in this study could create large pores with an improved cell infiltration across the assembled constructs.

With the established electrospinning conditions [8, 20], PCL/collagen (3:1 w/w) blends could be electrospun into nanofibers with the fiber diameter of 300-600 nm. Such nanofiber mats supports the adhesion and proliferation of various cells [8, 32]. Depending on the configuration of the collector, fibers in electrospun mats can take various organizations, *e.g.*, anisotropic or isotropic, which significantly relies on the distribution of electric field between the spinneret and the grounded surface. For the grounded flat surface with a uniform “0” potential, the fibers have a relative equal opportunity to deposit onto the collecting surface, which leads to the isotropic random fiber organization (Fig. 4A, D and G). For the grounded rotating mandrel, the

circumference of the mandrel has an equal "0" potential, and the shortest distance between spinneret and tangible surface of mandrel determines the preferred deposition of fibers onto this area first, and then pulled to align along the rotation direction at a high rotation speed. As a result, fiber mats with uniaxial fiber orientation are obtained [20, 33, 34] (Fig. 4B, E and H). For both cases, the fiber spatial density, especially the inter-fiber distance would be comparable across the fiber mats. To obtain the fiber mats with uneven fiber distribution, manipulation of the electric field distribution between the spinneret and the collection surface would be an effective approach, which can be achieved by either creating patterned domains on the collection surface with varying distances to the spinneret or creating patterned domains with different potentials. In this study, the use of stainless steel mesh as fiber collection surface could create a patterned potential distribution, *i.e.*, conductive wires separated by non-conductive void space (Fig. 1A&B), and meanwhile the up-and-down curved metal wires also led to a distance variation to the spinneret (Fig. 1A). As a result, a high density of PCL/collagen nanofibers accumulated on the metal wires while some loose and cross-aligned fibers depositing in the void areas (Fig. 2A&C). The formation of cross-aligned fibers across the void space is ascribed to the preferred fiber deposition onto parallel adjacent upper metal wires at the same height. Such a unique fiber organization introduced patterns to nanofiber mats with periodic alteration of the inter-fiber pore size. Upon prolonging the spinning time, continuous deposition of nonconductive PCL/collagen nanofibers onto the metal wire surface gradually reduces the electric field difference, accounting for the deposition of more random fibers in the void area with reduced pore size (Table 2). Large interfiber pore size is always favorable for cell infiltration, but can compromise the mechanical strength. In this study, the spinning time of 25 sec seems optimal to satisfy both better cell infiltration (approximately 19-μm pore size) and better mechanical strength (5MPa).

Further characterization of cell infiltration through multilayers of mesh-patterned nanofiber mats did find more cells presented in the middle of the stacked fiber mats, significantly higher than that with either random or aligned fiber mats (Fig. 6). Theoretically, it is possible for the cells to pass through the entire thickness of stacked fiber mats if the loose fiber areas (*i.e.*, the void zone) of patterned nanofiber mats are perfectly aligned. On the other hand, the penetration depth with present patterned nanofiber mats (25 sec) would be sufficient for the cells to cross the layers to form an integrated structure. The vertical orientation of fibroblasts in the assembled 3D constructs of cell-seeded patterned nanofiber mats (Fig. 7D) confirms that large pores indeed favor the fibroblasts migration through various layers.

Two distinct cell morphologies (stellate and elongated) were simultaneously and repeatedly observed with the fibroblasts cultured on patterned nanofiber mats (Fig. 5F and 5G). Our previous results showed that cell morphology on nanofibers is closely controlled by the organization of underneath nanofibers, regulating the formation and distribution of focal adhesion complexes (*e.g.*, vinculins) and consequently inducing the intracellular organization of cytoskeletal proteins (*e.g.*, F-actin and microtubulins) [28, 32]. As reported, randomly oriented nanofibers normally induce small and evenly distributed focal adhesion contact points in the circumferential edge of the fibroblasts while aligned fibers induce long and polarized focal adhesion point formation along the aligned fibers [28]. In the patterned nanofiber mats, three distinct nanofiber organizations were observed, *i.e.*, random, aligned and cross-aligned (Fig. 2). In this case, it is not a surprise to see varying cell morphologies within the same patterned fiber mat. Our ongoing efforts are made to investigate whether such a cell morphology variation can induce differential cell phenotype [28, 35].

Stacking cell-seeded nanofiber mats layer-by-layer allows the assembly of various cells with different nanofibers into a 3D construct with a potential to mirror the heterogeneity of native skin [8]. The large pores of patterned nanofiber mats support cell infiltration to form an integrated structure, however, with more layers stacked up, limited supply of nutrients to the interior cells may cause cell devitalization and lead to layer separation especially upon prolonged culture. To address this challenge, two possible approaches can be taken, including 1) acceleration of medium flow through the layers for better mass exchange by stirring, or 2) introduction of vasculature networks into the constructs while cell/nanofiber assembly [8, 28, 32]. The latter one represents a long-term solution, especially for timely vascularization upon *in vivo* transplantation of the cultured constructs in a fashion similar to autologous grafts [36]. As a matter of fact, the absence of a vascular network in 3D engineered tissues with densely populated cells can rapidly develop a necrotic core [37]. In recognition, part of our ongoing efforts is also focused on the formation of 3D vascularized constructs.

5. Conclusion

In the present study, metal mesh-patterned nanofiber mats with periodic alteration of fiber density and organizations were fabricated and evaluated for their efficiency in forming the integrated 3D constructs. With large interfiber pores formed among less dense fibers, cell infiltration through the patterned nanofiber mats was significantly improved and led to a better integration of layers in the assembled constructs of cell-seeded patterned nanofiber mats. Taken together, the metal mesh-patterned nanofiber mats show their advantages in promoting cell infiltration for better formation of 3D tissues.

Acknowledgement

The authors are grateful for the technical assistance from Mr. Chao Jia in fluorescence imaging. Part of the work was financially supported by NSF-IIP (1338958, 1346430, Wang), NSF-DMR (1508511, Wang), NSF-CBET (1033742, Wang), NIAMS (1R21 AR056416, Wang). Mr. Seyed Babak Mahjour was supported by the Innovation & Entrepreneurship Doctoral Fellowship from Stevens Institute of Technology.

References:

1. Madison KC. Barrier function of the skin: "la raison d'être" of the epidermis. J. Invest. Dermatol. 2003;121(2):231-41.
2. Holbrook KA, Byers PH, Pinnell SR. The structure and function of dermal connective tissue in normal individuals and patients with inherited connective tissue disorders. Scan. Electron Microsc. 1982;(Pt 4):1731-44.
3. Vaz CM, van Tuijl S, Bouten CV, Baaijens FP. Design of scaffolds for blood vessel tissue engineering using a multi-layering electrospinning technique. Acta Biomater. 2005;1(5):575-82.
4. Orr SB, Chainani A, Hippensteel KJ, Kishan A, Gilchrist C, Garrigues NW, Ruch DS, Guilak F, Little D. Aligned multilayered electrospun scaffolds for rotator cuff tendon tissue engineering. Acta Biomater. 2015;24:117-26.
5. Steele JA, McCullen SD, Callanan A, Autefage H, Accardi MA, Dini D, Stevens MM. Combinatorial scaffold morphologies for zonal articular cartilage engineering. Acta Biomater. 2014;10(5):2065-75.
6. Yan Y, Xiong Z, Hu Y, Wang S, Zhang R, Zhang C. Layered manufacturing of tissue engineering scaffolds via multi-nozzle deposition. Materials Letters. 2003;57(18): 2623–2628.

7. Delcroix GJR, Molinari M, Reiner T, Temple HT, Valdes M, Montero RB, Andreopoulos FM, Schiller PC, D'Ippolito G. Multi-Layered Scaffold to Mimic Hyaline Articular Cartilage Architecture. Current Tissue Engineering 2015; 4 (2)(E-pub ahead of print).
8. Yang X, Shah J, Wang H. Nanofiber enabled layer-by-layer approach toward three-dimensional tissue formation. Tissue Eng. Part A 2009;15:945-956.
9. Sill TJ, von Recum HA. Electrospinning: applications in drug delivery and tissue engineering. Biomaterials 2008;29:1989-2006.
10. Yoo HS, Kim TG, Park TG. Surface-functionalized electrospun nanofibers for tissue engineering and drug delivery. Adv. Drug. Deliv. Rev. 2009;61:1033-1042.
11. Chen X, Fu X, Shi G, Wang H. Regulation of the osteogenesis of preosteoblasts by nanofiber spatial arrangement in 2D and 3D environments. Nanomedicine 2013;9:1283-1292.
12. Wang K, Xu M, Zhu M, Su H, Kong D, Wang H, Wang L. Creation of macropores in electrospun silk fibroin Scaffolds using sacrificial PEO-microparticles to improve cellular infiltration. J. Biomed. Mater. Res. A. 2013;101:3474-3481.
13. Lee YH, Lee JH, An IG, Kim C, Lee DS, Lee YK, Nam JD. Electrospun dual-porosity structure and biodegradation morphology of montmorillonite reinforced PLLA nanocomposite scaffolds. Biomaterials 2005; 26:3165–3172.
14. Kim TG, Chung HJ, Park TG. Macroporous and nanofibrous hyaluronic acid/collagen hybrid scaffold fabricated by concurrent electrospinning and deposition/leaching of salt particles. Acta Biomater. 2008;4:1611-1619.
15. Nam J, Huang Y, Agarwal S, Lannuntti J. Improved celllular infiltration in electrospun fiber via engineered porosity. Tissue Eng. 2007;13:2249-2257.

16. Wulkersdorfer B, Kao KK, Agopian VG, Ahn A, Dunn JC, Wu BM, Stelzner M. Bimodal porous scaffolds by sequential electrospinning of poly(glycolic acid) with sucrose particles. Int. J. Polym. Sci. 2010; 4:36178.

17. Lee JB, Jeong SI, Bae MS, Yang DH, Heo DN, Kim CH, Alsberg E, Kwon IK. Highly porous electrospun nanofibers enhanced by ultrasonication for improved cellular infiltration. Tissue Eng. Part A 2011;17:2695-2702.

18. Neves N, Campos R, Pedro A, Reis R. Patterning of polymer nanofiber meshes by electrospinning for biomedical applications. Int. J. Nanomedicine 2007; 2:433-438.

19. Wang Y, Wang G, Chen L, Li H, Yin T, Wang B, Lee JC, Yu Q. Electrospun nanofiber meshes with tailored architectures and patterns as potential tissue-engineering scaffolds. Biofabrication 2009;1:5001-5010.

20. Yang X, Wang H. Electrospun functional nanofibrous scaffolds for Tissue Engineering In: Eberli, D, editor. Tissue Eng. 2010. p 159-178.

21. Yang D, Zhang J, Zhang J, Nie J. Aligned electrospun nanofibers induced by magnetic field. J. Appl. Polym. Sci. 2008;110:3368-3372.

22. Jia C, Yu D, Lamarre M, Leopold P, Teng YD, Wang H. Patterned electrospun nanofiber matrices via localized dissolution: potential for guided tissue formation. Adv. Mater. 2014;26:8192-8197.

23. Li D, Wang Y, Xia Y. Electrospinning nanofibers as uniaxially aligned arrays and layer-by-layer stacked films. Adv. Mater. 2004;16:361-366.

24. Xie J, Liu W, MacEwan MR, Bridgman PC, Xia Y. Neurite outgrowth on electrospun nanofibers with uniaxial alignment: the effects of fiber density, surface coating, and supporting substrate. ACS nano 2014;8:1878-1885.

25. Li D, Quyang G, McCann JT, Xia Y. Collecting electrospun nanofibers with patterned electrodes. Nano Lett 2005;5: 913-916.

26. Liu W, Thomopoulos S, Xia Y. Electrospun nanofibers for regenerative medicine. Adv. Healthc. Mater. 2012;1:10-25.

27. Wang H, Van Blitterswijk CA, Bertrand-De Hass M, Schuurman AH. Improved enzymatic isolation of fibroblasts for the creation of autologous skin substitutes In Vitro. Cell Dev. Biol. 2004;40:268-277.

28. Huang C, Fu X, Liu J, Qi Y, Li S, Wang H. The involvement of integrin β1 signaling in the migration and myofibroblastic differentiation of skin fibroblasts on anisotropic collagen-containing nanofibers. Biomaterials 2012;33:1791-1800.

29. Kim TG, Shin H, Lim DW. Biomimetic scaffolds for tissue engineering. Adv. Funct. Mater. 2012;22:2446-2468.

30. Yang F, Murugan R, Wang S, Ramakrishna S. Electrospinning of nano/micro scale poly (l-lactic acid) aligned fibers and their potential in neural tissue engineering. Biomaterials 2005;26:2603-2610.

31. Sefat F, Denyer MC, Youseffi M. Imaging via widefield surface plasmon resonance microscope for studying bone cell interactions with micropatterned ECM proteins. Microscopy 2010;241:282-290.

32. Mahjour SB, Ghaffarpasand F, Wang H. Hair follicle regeneration in skin grafts: current concepts and future perspectives. Tissue Eng. Part B 2012;18:15-23.

33. Cai S, Xu H, Jiang Q, Yang Y. Novel 3D electrospun scaffolds with fibers oriented randomly and evenly in three dimensions to closely mimic the unique architectures of

extracellular matrices in soft tissues: fabrication and mechanism study. Langmuir 2013;29:2311-2318.

34. Yang F, Murugan R, Wang S, Ramakrishna S. Electrospinning of nano/micro scale poly(L-lactic acid) aligned fibers and their potential in neural tissue engineering. Biomaterials 2005;26:2603-2610.
35. Tsimbouri P, Gadegaard N, Burgess K, White K, Reynolds P, Herzyk P, Oreffo R, Dalby MJ. Nanotopographical effects on mesenchymal stem cell morphology and phenotype. J. Cell. Biochem. 2014;115(2):380-90.
36. Sheridan RL, Morgan JR, Cusick JL, Petras LM, Lydon MM, Tompkins RG. Initial experience with a composite autologous skin substitute. Burns 2001;27:421-424.
37. Radisic M, Yang L, Boublik J. Medium perfusion enables engineering of compact and contractile cardiac tissue. Am. J. Physiol. 2004;286:507–516.

List of Figures:

Figure 1. Simulation of the electric potential distribution between the spinneret and the grounded metal mesh using the COMSOL-multiphysics software. (A) Schematic illustration of the typical electrospinning setup for patterned nanofiber mats using the stainless steel wire mesh as the fiber collector. (B) Micrographs of the metal mesh with the dimensions. (C) Slice view of the electric potential between spinneret and grounded metal mesh. (D) Zoom-in slice view of the potential distribution across the metal wire mesh area.

Figure 2. Patterned electrospun PCL/collagen nanofiber mats collected on the metal wire mesh for 25 seconds. SEM examination of the collected fiber mats (A) showed 4 typical zones with distinct fiber density and organization (B-E): Zone 1 shows the fibers collected on the void space of the mesh while Zones 2, 3 and 4 show the fibers collected either on the protruded wire (4) or dented wires (2 and 3). (A): scale bar= 1mm; (B-E): scale bar= 5 μm. The pore size and fiber organization for each zone were summarized in Table 1.

Figure 3. Time-dependent collection of patterned electrospun PCL/collagen nanofiber mats on the metal wire meshes for 10 (A, E, I), 20 (B, F, J), 30 (C, G, K), and 40 (D, H, L) seconds. The fiber mats were examined either under the phase contrast microscope (A-H) or under SEM (I-L). (A-D): scale bar=2 mm; (E-H): scale bar=200 μm; (I-L): scale bar=20 μm.

Figure 4. Electrospun nanofiber mats with various fiber organizations using different setup. Schematic illustration of the setup for fabricating random (A), aligned (B), and patterned (C) electrospun nanofibers. Representative micrographs of various electrospun PCL/collagen nanofiber mats with random (D, G, J), aligned (E, H, K) or patterned (F, I, L) fiber arrangements. The fiber mats were examined either under the phase contrast microscope (D-F) or under SEM (G-L). (D-F): scale bar=100 μm; (G-I): scale bar=2 μm; (J-L): scale bar=400 nm.

Figure 5. Representative micrographs of fibroblasts (passage 1) cultured on various electrospun PCL/collagen nanofiber mats with random (A, D), aligned (B, E) or patterned (C, F, G) fiber arrangements for 7 days. (A-C) Phase contrast microscopic images of fibroblasts after methylene blue staining. Scale bar=150 μm. (D-G) Fluorescent staining of intracellular cytoskeleton protein of F-actin (red) with phalloidin-TRITC and nuclei (blue) with DAPI. Scale bar=100 μm. Double-head broken line indicates the alignment direction.

Figure 6. (A) Schematic illustration of the experimental setup for cell penetration study, in which fibroblasts (at a density of $8 \times 10^3/cm^2$) were seeded onto the stack of 15 layers of nanofiber mats. (B-D) Representative micrographs of the cross-section of the cell-seeded constructs cultured for 14 days after hematoxylin and eosin (H&E) staining. Scale bar=100 μm. Yellow arrows indicate the cells. Cell penetration depth into each type of nanofiber mat stacks (n=5) was measured based on the H&E stained sections and summarized in Table 4.

Figure 7. (A) Schematic illustration of the nanofiber-enabled layer-by-layer cell assembly, in which cell-seeded nanofiber mats were stacked on top of each other to form 3D constructs. Representative micrographs of the H&E stained cross-sections of the multilayered fibroblast-nanofiber constructs with random (B), aligned (C) or patterned (D) fiber arrangement. 15 layers

of fibroblast-seeded nanofiber mats (at a density of $8 \times 10^3/cm^2$) were stacked and cultured for 14 days. Scale bar = 100 μm. White arrows indicate the horizontally oriented cell nuclei and yellow arrows indicate the vertically oriented cell nuclei.

List of Tables:

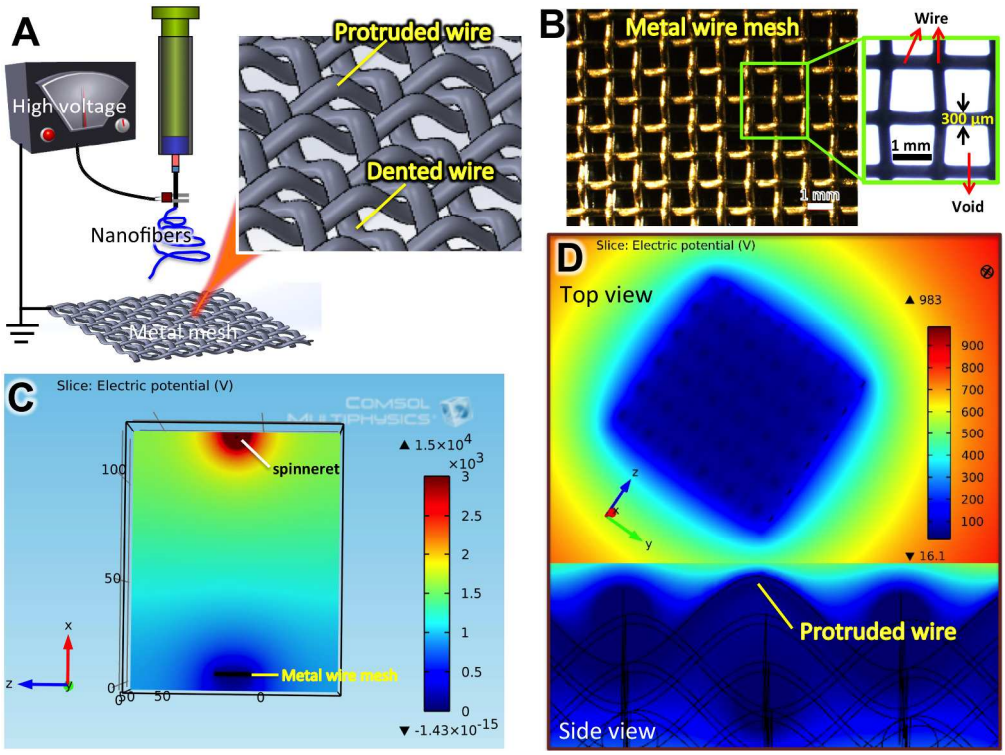

Figure 1. Simulation of the electric potential distribution between the spinneret and the grounded metal mesh using the COMSOL-multiphysics software. (A) Schematic illustration of the typical electrospinning setup for patterned nanofiber mats using the stainless steel wire mesh as the fiber collector. (B) Micrographs of the metal mesh with the dimensions. (C) Slice view of the electric potential between spinneret and grounded metal mesh. (D) Zoom-in slice view of the potential distribution across the metal wire mesh area.
1040x776mm (72 x 72 DPI)

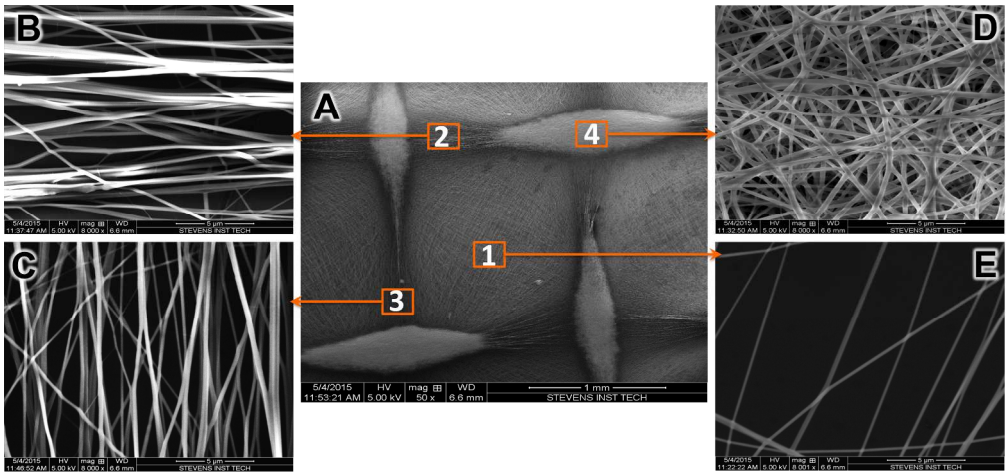

Table 1. Pore size and fiber spatial organization of wire-patterned nanofibrous mats

Zone	1	2	3	4
Pore size (μm)	19.3± 1.8	1.9± 0.5	2.3± 0.6	0.3± 0.1
Fiber organization	Cross-aligned	aligned	aligned	random

Figure 2. Patterned electrospun PCL/collagen nanofiber mats collected on the metal wire mesh for 25 seconds. SEM examination of the collected fiber mats (A) showed 4 typical zones with distinct fiber density and organization (B-E): Zone 1 shows the fibers collected on the void space of the mesh while Zones 2, 3 and 4 show the fibers collected either on the protruded wire (4) or dented wires (2 and 3). (A): scale bar= 1mm; (B-E): scale bar= 5 μm. The pore size and fiber organization for each zone were summarized in Table 1.
975x609mm (72 x 72 DPI)

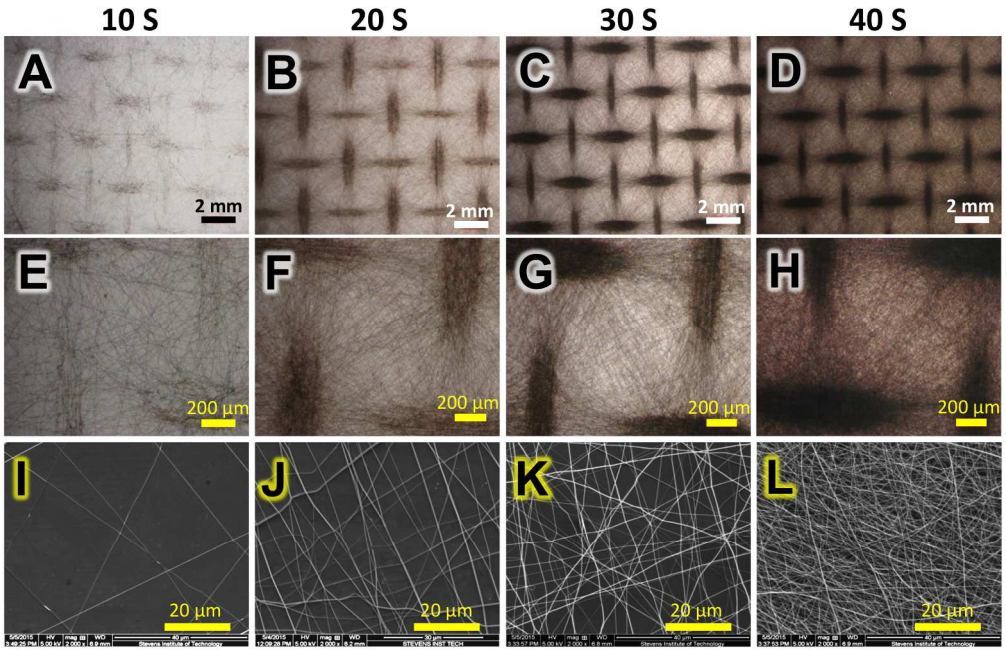

Figure 3. Time-dependent collection of patterned electrospun PCL/collagen nanofiber mats on the metal wire meshes for 10 (A, E, I), 20 (B, F, J), 30 (C, G, K), and 40 (D, H, L) seconds. The fiber mats were examined either under the phase contrast microscope (A-H) or under SEM (I-L). (A-D): scale bar=2 mm; (E-H): scale bar=200 µm; (I-L): scale bar=20 µm.
868x557mm (72 x 72 DPI)

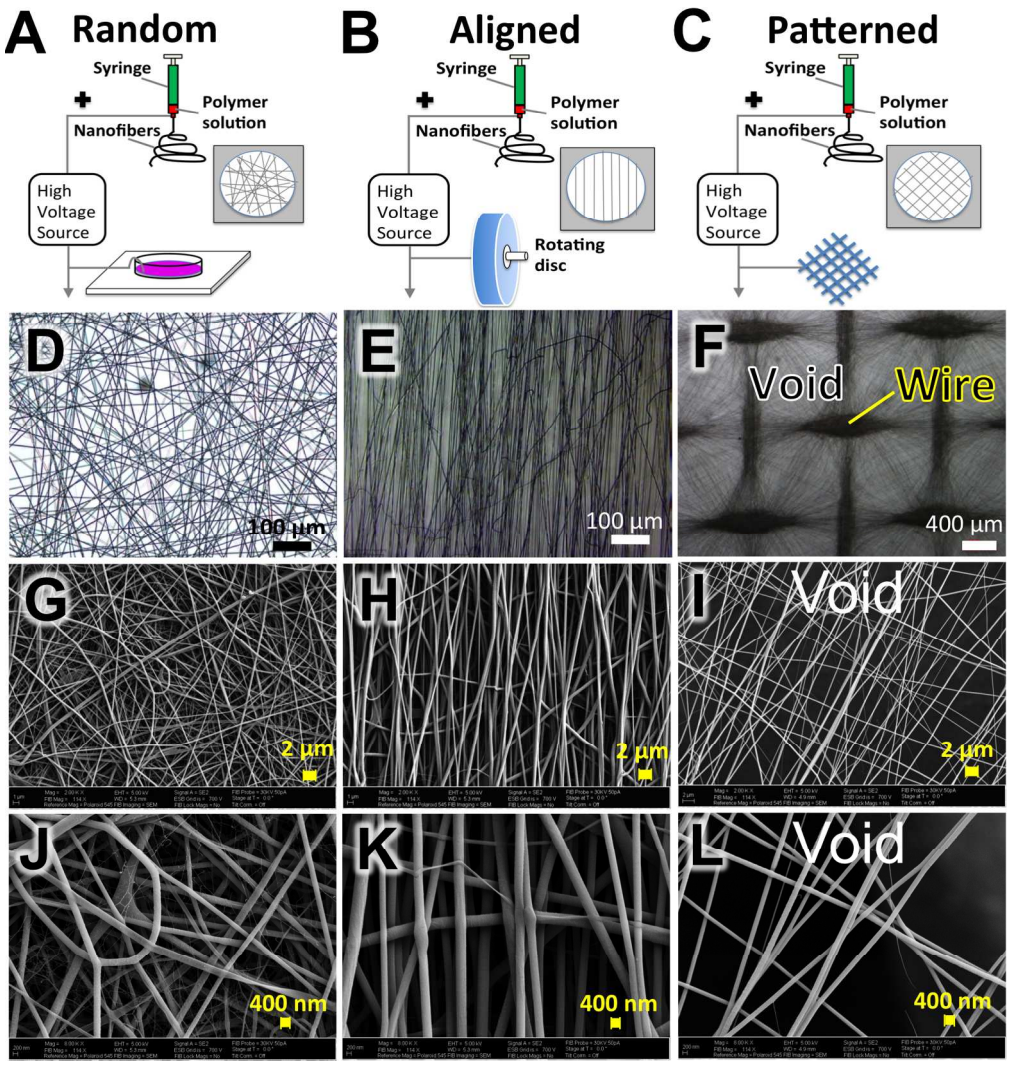

Figure 4. Electrospun nanofiber mats with various fiber organizations using different setup. Schematic illustration of the setup for fabricating random (A), aligned (B), and patterned (C) electrospun nanofibers. Representative micrographs of various electrospun PCL/collagen nanofiber mats with random (D, G, J), aligned (E, H, K) or patterned (F, I, L) fiber arrangements. The fiber mats were examined either under the phase contrast microscope (D-F) or under SEM (G-L). (D-F): scale bar=100 µm; (G-I): scale bar=2 µm; (J-L): scale bar=400 nm.
700x736mm (72 x 72 DPI)

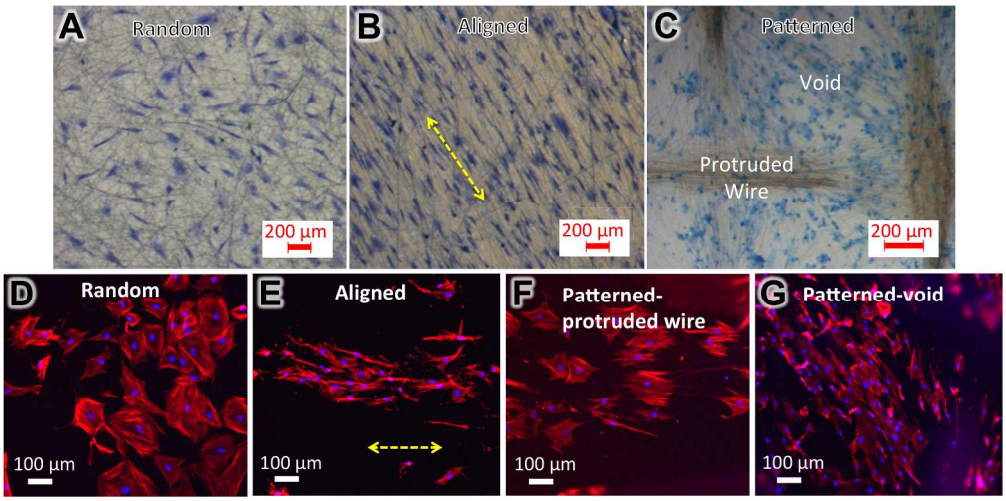

Figure 5. Representative micrographs of fibroblasts (passage 1) cultured on various electrospun PCL/collagen nanofiber mats with random (A, D), aligned (B, E) or patterned (C, F, G) fiber arrangements for 7 days. (A-C) Phase contrast microscopic images of fibroblasts after methylene blue staining. Scale bar=150 µm. (D-G) Fluorescent staining of intracellular cytoskeleton protein of F-actin (red) with phalloidin-TRITC and nuclei (blue) with DAPI. Scale bar=100 µm. Double-head broken line indicates the alignment direction.
972x476mm (72 x 72 DPI)

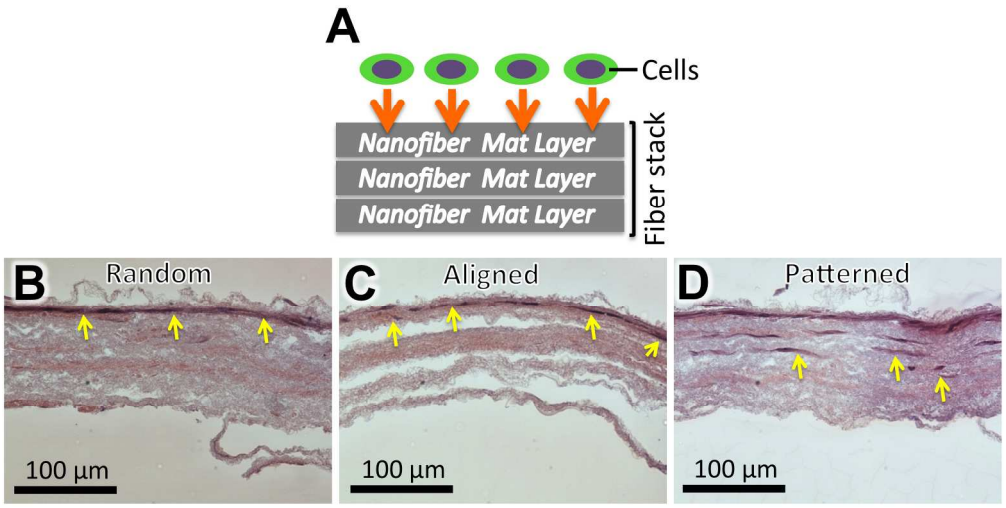

Figure 6. (A) Schematic illustration of the experimental setup for cell penetration study, in which fibroblasts (at a density of 8 × 103/cm2) were seeded onto the stack of 15 layers of nanofiber mats. (B-D) Representative micrographs of the cross-section of the cell-seeded constructs cultured for 14 days after hematoxylin and eosin (H&E) staining. Scale bar=100 µm. Yellow arrows indicate the cells. Cell penetration depth into each type of nanofiber mat stacks (n=5) was measured based on the H&E stained sections and summarized in Table 4.
861x430mm (72 x 72 DPI)

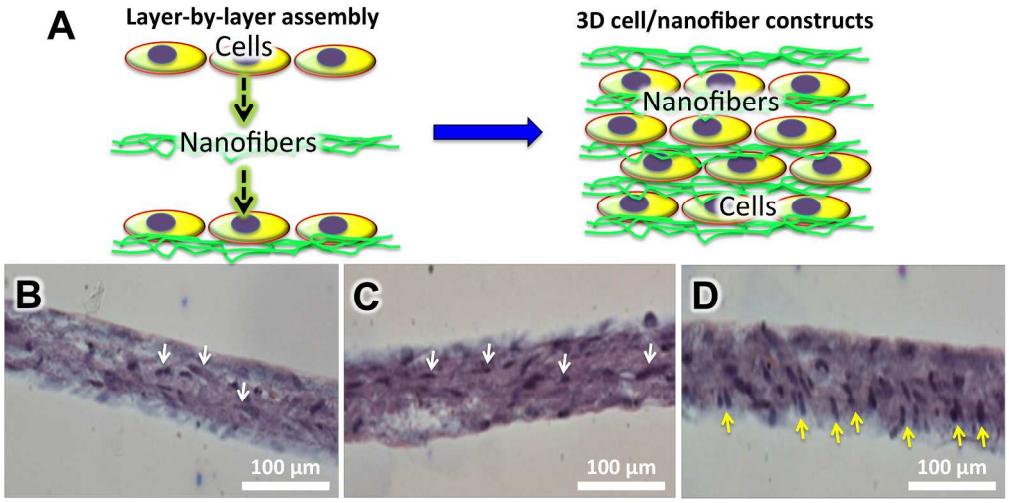

Figure 7. (A) Schematic illustration of the nanofiber-enabled layer-by-layer cell assembly, in which cell-seeded nanofiber mats were stacked on top of each other to form 3D constructs. Representative micrographs of the H&E stained cross-sections of the multilayered fibroblast-nanofiber constructs with random (B), aligned (C) or patterned (D) fiber arrangement. 15 layers of fibroblast-seeded nanofiber mats (at a density of 8 × 103/cm2) were stacked and cultured for 14 days. Scale bar = 100 µm. White arrows indicate the horizontally oriented cell nuclei and yellow arrows indicate the vertically oriented cell nuclei.
1048x515mm (72 x 72 DPI)

Table 1. Pore size and fiber spatial organization of the wire-patterned nanofiber mats.

Zone	1	2	3	4
Pore Size (μm)	19.3 ± 1.8	1.9 ± 0.5	2.3 ± 0.6	0.3 ± 0.1
Fiber Organization	Cross-aligned	Aligned	Aligned	Random

Table 2. Key attributes of patterned nanofiber mats in relation to spinning time from 10 to 40 seconds.

Spinning Time (Seconds)	10	20	25	30	40
Pore Size (μm)	33.21 ± 5.1	24.3 ± 2.4	19.3 ± 1.8	11.1 ± 1.9	0.9 ± 0.4
Pass-through Cells	5134 ± 105	3752 ± 86	2458 ± 62	112 ± 10	10 ± 1
Tensile Strength at Breaking (MPa)	2.3 ± 0.6	4.5 ± 0.1	5.0 ± 0.4	6.3 ± 0.5	7.0 ± 0.2

Table 3. Key parameters (fiber diameter, pore size, pass-through cells) of various nanofiber mats.

Nanofiber Mat	**Random**	**Aligned**	**Patterned**
Fiber Diameter (nm)	535 ± 85	499 ± 80	435± 78
Pore Size (μm)	1.6 ± 0.8	2.4± 0.6	19.3 ± 1.8
Pass-through Cells	5 ± 1	104 ± 11	2870 ± 96

Table 4. Cell penetration depth into the stacks of 15 layers of fiber mats.

Nanofiber Mat	**Random**	**Aligned**	**Patterned**
Infiltration Depth (μm)	2.2 ± 0.5	4.1 ± 0.7	35.4 ± 8.8